

Article

Photonic Crystals with a Defect Fabricated by Two-Photon Polymerization for the Infrared Spectral Range

Victoria Paige Stinson ^{*}, Serang Park, Micheal McLamb, Glenn Boreman and Tino Hofmann

Department of Physics and Optical Science, University of North Carolina at Charlotte, 9201 University Blvd, Charlotte, NC 28223, USA; spark71@uncc.edu (S.P.); mmclam10@uncc.edu (M.M.); gboreman@uncc.edu (G.B.); tino.hofmann@uncc.edu (T.H.)

* Correspondence: vstinso1@uncc.edu

Abstract: One-dimensional photonic crystals composed of alternating layers with high- and low-density were fabricated using two-photon polymerization from a single photosensitive polymer for the infrared spectral range. By introducing single high-density layers to break the periodicity of the photonic crystals, a narrow-band defect mode is induced. The defect mode is located in the center of the photonic bandgap of the one-dimensional photonic crystal. The fabricated photonic crystals were investigated using infrared reflection measurements. Stratified-layer optical models were employed in the design and characterization of the spectral response of the photonic crystals. A very good agreement was found between the model-calculated and measured reflection spectra. The geometric parameters of the photonic crystals obtained as a result of the optical model analysis were found to be in good agreement with the nominal dimensions of the photonic crystal constituents. This is supported by complimentary scanning electron microscope imaging, which verified the model-calculated, nominal layer thicknesses. Conventionally, the accurate fabrication of such structures would require layer-independent print parameters, which are difficult to obtain with high precision. In this study an alternative approach is employed, using density-dependent scaling factors, introduced here for the first time. Using these scaling factors a fast and true-to-design method for the fabrication of layers with significantly different surface-to-volume ratios. The reported observations furthermore demonstrate that the location and amplitude of defect modes is extremely sensitive to any layer thickness non-uniformities in the photonic crystal structure. Considering these capabilities, one-dimensional photonic crystals engineered with defect modes can be employed as narrow band filters, for instance, while also providing a method to quantify important fabrication parameters.



Citation: Stinson, V.P.; Park, S.; McLamb, M.; Boreman, G.; Hofmann, T. Photonic Crystals with a Defect Fabricated by Two-Photon Polymerization for the Infrared Spectral Range. *Optics* **2021**, *2*, 284–291. <https://doi.org/10.3390/opt2040027>

Academic Editor: Yuriy Garbovskiy

Received: 26 October 2021

Accepted: 13 November 2021

Published: 6 December 2021

Publisher's Note: MDPI stays neutral with regard to jurisdictional claims in published maps and institutional affiliations.



Copyright: © 2021 by the authors. Licensee MDPI, Basel, Switzerland. This article is an open access article distributed under the terms and conditions of the Creative Commons Attribution (CC BY) license (<https://creativecommons.org/licenses/by/4.0/>).

Keywords: photonic crystal; two-photon polymerization; defect mode; layer thickness non-uniformity

1. Introduction

Photonic crystals are capable of providing nearly perfect reflection in a narrow spectral window, referred to as the photonic bandgap, which can be easily tuned for a desired spectral range by tailoring the constituents of the photonic crystal [1–15]. The early motivation for the development of photonic crystals was centered around their unique applications in quantum electronics and quantum optics [16]. Photonic crystals can be categorized as one-, two-, and three-dimensional, depending on the spatial arrangement of constituents of the photonic crystals, which determine their application [17]. One-dimensional photonic crystals are the simplest of these geometries and these can be realized through the periodic arrangement of transparent layers with different dielectric properties [1,2,4–7,11–14,17].

It has been demonstrated that defects in the spatially periodic arrangement of the dielectric layers induce defective states in the photonic bandgap, which can result in narrow transmission bands within a band of high reflectivity [4–7,13,14,17]. For one-dimensional photonic crystals, a defect mode can be introduced via the addition of a layer which disrupts the dielectric periodic arrangement of the surrounding layers. Such photonic crystals

have been designed for several applications, including enhanced Faraday rotators [4], omnidirectional bandgap filters [5], sensors [18,19], and narrow band filters [20].

Several techniques have been demonstrated for the fabrication of one-dimensional photonic crystals. The most commonly used method is spin coating, which allows the fabrication of sequences of thin films with different dielectric properties [10,21]. Other methods include self-assembly, which uses a layer-by-layer approach, top-down etching, chemical vapor deposition, physical vapor deposition, and molecular beam epitaxy [10,22]. Direct laser writing using two-photon polymerization has been recently used to fabricate photonic crystals [9,11,23]. One of the main advantages of two-photon polymerization is its capability to synthesize virtually arbitrary geometries with critical dimensions on the order of a few hundred nanometers. This enables the fabrication of photonic crystals from a single dielectric material using alternating layers of high- and low-density [11]. The scale of photonic crystals fabricated by means of two-photon polymerization is often limited due to the serial nature of the two-photon polymerization process, which can lead to extensive fabrication times. Novel approaches have aimed for the acceleration of the fabrication process by combining traditional interference lithography and two-photon lithography [24]. Using this approach, three-dimensional photonic crystals with controlled defects have very recently been demonstrated.

The accuracy by which structures can be fabricated using the two-photon polymerization approach is greatly affected by the choice of the focusing objective and the fabrication parameters used, such as laser power, scan speed [25–27], and laser-beam paths governed by slicing and hatching distances [28]. Any of these parameters will affect the volume over which polymerization occurs. The voxel size of the instrument depends on a wide range of parameters and therefore can alter the fabricated sample geometry. Although the power density is determined by the scan speed and the nominal laser power, the slicing and hatching distance will affect the resolution and integrity of features in the horizontal plane and the vertical plane, respectively [28]. Determining the optimal settings for these parameters is indispensable in order to achieve a desired spectral response.

The position of the photonic bandgap in a one-dimensional photonic crystal is sensitive even to small changes in thickness (± 5 nm), as well as changes in the dielectric properties of its constituent layers [11]. Thus, it is critical to determine fabrication parameters which result in a true-to-design geometry with minimal variation in the layer thickness and dielectric properties across the constituent layers.

In this paper, we demonstrate the successful fabrication of one-dimensional photonic crystals with defects that induce narrow transmission bands centered within the photonic bandgap using two-photon polymerization from a single monomer. Experimental data and stratified-layer optical model calculations reveal that the induced defect modes are extremely sensitive to the layer thickness uniformity of the photonic crystal. In addition, a simple approach for the optimization of two-photon polymerization fabrication parameters for photonic crystals is introduced. Our proposed approach introduces a geometric scaling factor, which helps to obtain the true-to-design fabrication of photonic crystals, while substantially reducing the time required to determine optimal fabrication parameters.

2. Design, Fabrication, and Characterization

One-dimensional photonic crystals composed of alternating layers of high- and low-density (see Figure 1) were designed using stratified-layer optical model calculations (WVASE32, J.A. Woollam, Co., Lincoln, NE, USA). Alternating dielectric layers were produced using a two-photon polymerization-compatible polymer IP-Dip. The dielectric properties of the compact layers $\epsilon^{\text{IP-Dip}}(\omega)$ are described by means of the parameterized model-dielectric-function of polymerized IP-Dip. The model-dielectric-function of this material has been previously established using spectroscopic ellipsometry in the infrared spectral range and is described using a simple mixed oscillator model [29].

The low-density layers consist of sub-wavelength cylindrical pillars which are arranged in a square lattice pattern and are oriented normal to the low-density/high-density

interface. The dielectric function of the low-density layers $\epsilon_{\text{low}}^{\text{eff}}(\omega, f_i)$ can be described using the Bruggeman effective medium approximation given by [30]:

$$\epsilon_{\text{low}}^{\text{eff}}(\omega, f_i) = \frac{1}{4} \left\{ (3f_i - 1)\epsilon_i(\omega) + (2 - 3f_i)\epsilon_h(\omega) \pm \left([(3f_i - 1)\epsilon_i(\omega) + (2 - 3f_i)\epsilon_h(\omega)]^2 + \epsilon_i(\omega)\epsilon_h(\omega) \right)^{\frac{1}{2}} \right\}. \quad (1)$$

The dielectric properties of the inclusions and the host medium are then given by ϵ_i and ϵ_h , respectively. In our design the host medium is air, i.e., $\epsilon_h = 1$, whereas the inclusions consist of polymerized IP-Dip $\epsilon_i(\omega) = \epsilon^{\text{IP-Dip}}(\omega)$. The volume ratio between the cylindrical inclusions and the host medium is described by the volumetric fill factor f_i .

The effect of a high-density defect layer is explored by comparing the infrared optical response of two photonic crystals. Using simple stratified-layer optical model calculations, the photonic bandgaps of the photonic crystals are designed to be centered at $\omega = 2556 \text{ cm}^{-1}$ ($\lambda = 3.91 \text{ }\mu\text{m}$). The selection of the wavelength for the photonic bandgaps is based on the dielectric function of IP-Dip, which offers a transparent window in the range from 2000 to 3000 cm^{-1} [29]. One crystal is composed of 6 alternating high- and low-density layers. The thicknesses of the high- and low-density layers are designed to be 3.3 μm and 2.8 μm , respectively, as shown in Figure 1. The volumetric fill factor f_i of the low-density layers is $f_i = 0.2$. The second crystal is identical to the first crystal except for the introduction of a high-density defect layer in the center of the layer stack. The high-density defect layer has a thickness of 5.3 μm and consists of compact polymerized IP-Dip. The base of both photonic crystals is designed to be 49.2 $\mu\text{m} \times 49.2 \mu\text{m}$.

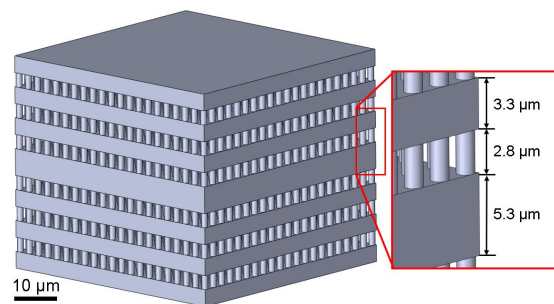


Figure 1. CAD model showing the dimensions of the one-dimensional photonic crystal design investigated here. The photonic crystal consists of alternating high-density, compact layers and low-density layers. The nominal thickness of the high-density layers is 3.3 μm . The low-density layers with a nominal thickness of 2.8 μm are composed of cylindrical pillars with a diameter of 1.2 μm , which are arranged in a square-lattice pattern on the surface with a lattice constant of 2.4 μm . The corresponding nominal volumetric fill factor f_i of the low-density layer is $f_i = 0.2$. For the photonic crystal with the high-density defect, the defect layer has a nominal thickness of 5.3 μm and is centered in the layer stack.

A commercial two-photon polymerization system (Photonic Professional GT, Nanoscribe, GmbH) was used to polymerize a single monomer (IP-Dip) in order to fabricate the one-dimensional photonic crystal structures on a fused silica substrate. It is very well known that the voxel size depends on a number of parameters, such as the objective, choice of monomer, laser power, scan speed, and hatching and slicing distances, for instance [25–28]. Thus, the identification of parameters which permit the true-to-design fabrication of complex structures can be difficult and time consuming.

For the photonic crystals discussed here, the volume-to-surface ratios between the low-density and high-density layers differ substantially. As a result, low- and high-density layers are affected differently by the solvent-diffusion-based swelling/contraction which occurs during the rinsing/drying process after the polymerization. This fabrication problem is resolved here by introducing a one-dimensional geometric scaling factor γ_{SF} , which pro-

vides a layer thickness scaling that is different for high- and low-density layers. The scaling factors were determined using photonic crystals without defects, but with otherwise identical designs. For the high-density layers $\gamma_{SF} = 0.92$ and for the low-density layers $\gamma_{SF} = 1.30$ was used.

Following the fabrication, the structures are rinsed in propylene glycol monomethyl ether acetate for 10 min, 99.99% isopropyl alcohol for 10 min, and then left to air dry for at least 30 min. A 63 \times objective lens with laser power at 20 mW and scan speed at 500 mm/s was used. Both slicing distance and hatching distance were set to 0.2 μm .

Infrared reflection measurements were carried out for all photonic crystals in the spectral range from 2000 cm^{-1} to 3000 cm^{-1} with a resolution of 2 cm^{-1} using an IR microscope (HYPERION 3000 Bruker, Inc., Billerica, MA, USA) in combination with an FTIR spectrometer (VERTEX 70, Bruker, Inc.). An IR microscope with an annular collection aperture was equipped with a Mercury-Cadmium-Telluride detector. A 15 \times Cassegrain objective with confocal illumination was used with an aperture setting of 20 μm , resulting in an angular spread of 0.6 $^\circ$ with an average angle of incidence of 8.7 $^\circ$. All reflection measurements were normalized to a bulk gold sample using the same aperture settings as those employed during the sample data acquisition. A silicon carbide globar was used as a light source. All measurements were performed at room temperature. Stratified-layer optical model calculations obtained using WVASE32 (J.A. Woollam Co., Lincoln, NE, USA) were employed to analyze the reflection measurements. SEM images, shown in Figure 2 independently demonstrated the quality of the fabrication and the resulting true-to-design dimensions of the fabricated photonic crystal.

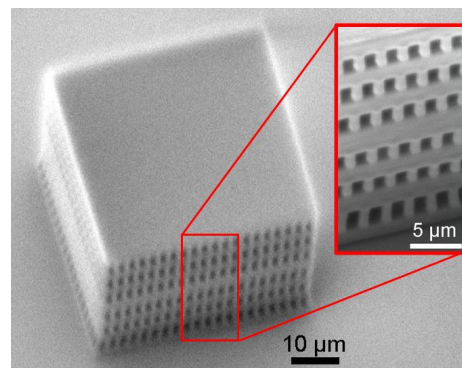


Figure 2. Scanning electron microscope (SEM) image taken at an operating voltage of 1 kV of the photonic crystal with a defect layer, as described by Figure 1. Inset SEM image taken with an operating voltage of 7 kV.

3. Results and Discussion

The experimental reflection data (dashed lines) and best-model calculated reflection data (solid lines) for both crystals are depicted in Figure 3. The major spectral feature is the photonic bandgap, which is centered at 2500 cm^{-1} for both photonic crystals. For the photonic crystals with the solid layer defect, a defect mode is formed in the center of the photonic bandgap. The reflection amplitude of the photonic crystal without a defect is 77%; with a high-density defect layer this amplitude is reduced to 62%. The defect mode of the photonic crystal with a high-density defect layer is centered at 2520 cm^{-1} and has a reflection amplitude of 26% with respect to the average bandgap maxima of 62%. A very good agreement was found between the best-fit stratified-layer optical model calculations (solid lines) and the experimental reflection measurements (dashed lines) for both photonic crystals.

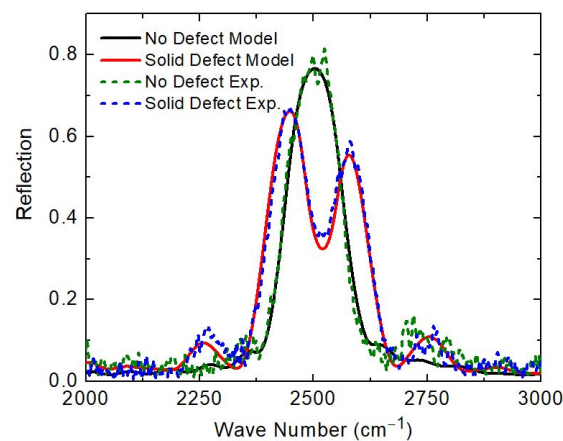


Figure 3. Comparison between best-model calculated (solid lines) and experimental (dashed lines) reflection data obtained from identical photonic crystals with and without a solid defect. The spectra were dominated by the photonic bandgap centered at approximately 2500 cm^{-1} . The photonic crystal with a solid defect exhibits a defect mode in the middle of the photonic bandgap. Experimental and best-model calculated data were in very good agreement.

The optical model is composed of 14 layers: a fused silica substrate, six A-B layer pairs of low- and high-density layers, and a high-density defect layer in the center, following the design shown in Figure 1. The dielectric functions of the glass substrate and IP-Dip used here were previously determined using spectroscopic ellipsometry and were not varied in the model [29,31]. Equation (1) is used to determine the dielectric function of the low-density layers. During the data analysis, geometrical model parameters were varied simultaneously, including: the layer thickness of the low- and high-density layers, layer thickness non-uniformity, and volumetric fill fraction f_i . All parameters were adjusted using a Levenberg–Marquardt-based algorithm until the best match between the model-calculated and experimental reflection data set was obtained. Note that the experimental data sets of both photonic crystals were analyzed simultaneously in order to reduce parameter correlations. The best-model thickness of the low-density layers was determined to be $(2.771 \pm 0.014)\ \mu\text{m}$, the high-density to be $(3.311 \pm 0.010)\ \mu\text{m}$, and the high-density defect layer to be $(5.240 \pm 0.015)\ \mu\text{m}$. The best-model volumetric fill factor was found to be $f_i = 0.296 \pm 0.007$. In order to model the experimental reflection data accurately, layer thickness non-uniformities were taken into account and found to be an average of $(2.8 \pm 0.1)\%$ for all layers.

The effect of this non-uniformity on the defect mode is illustrated in Figure 4, where stratified-layer optical model calculations for two photonic crystals with a defect are compared. The spectrum plotted with a black dashed line depicts the model-calculated reflection obtained assuming ideal interfaces and the red solid line assumes a 2.8% layer thickness non-uniformity. A photonic bandgap with a centered defect mode can be seen for both models; however, the amplitude of both the photonic bandgap and the defect mode is diminished for the photonic crystal with non-ideal interfaces. The reflection amplitude of the defect mode with perfect layer uniformity is 56%, whereas the amplitude with a 2.8% layer thickness non-uniformity is 26%. Additionally, the average photonic bandgap magnitude is reduced by approximately 5.6% with this non-uniformity present. Our experimental findings corroborate the theoretical calculations conducted by T.S. Perova et al. [8], which have shown that layer thickness non-uniformities induce a reduction in the bandgap amplitude similar to what is seen in Figure 4.

The influence of the layer thickness non-uniformity on the defect mode amplitude is shown in Figure 5. A comparison is made between the changes in the photonic bandgap amplitude in a photonic crystal without a defect and the defect mode amplitude in a photonic crystal with a defect with respect to layer thickness non-uniformity. The changes in amplitude are normalized to the maximum reflection of the photonic bandgap in the

photonic crystal with no defect and ideal, abrupt, plane-parallel interfaces. The change in amplitude of the defect mode is more significant for increasing layer thickness non-uniformity compared to that for the photonic bandgap. This trend continues up to a non-uniformity of 5% at which point the defect mode becomes indistinguishable.

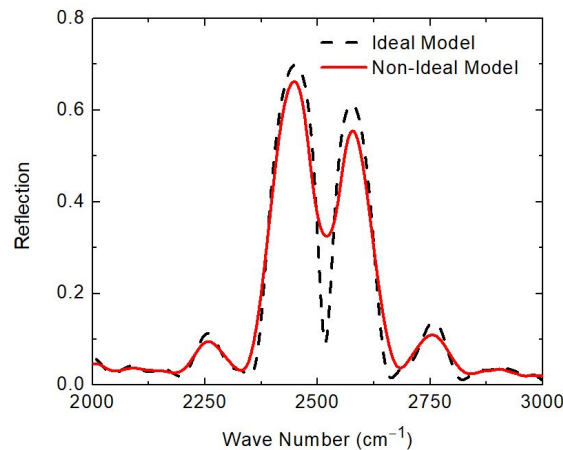


Figure 4. Model-calculated reflection data obtained for a stratified-layer model with ideal, plane parallel interfaces (black dashed line) in comparison to reflection data calculated using a model where a 2.8% layer thickness non-uniformity is assumed (red solid line). The largest difference can be observed at the defect mode resonance frequency, where the amplitude of the defect-mode is substantially suppressed after introducing layer thickness non-uniformity into the model.

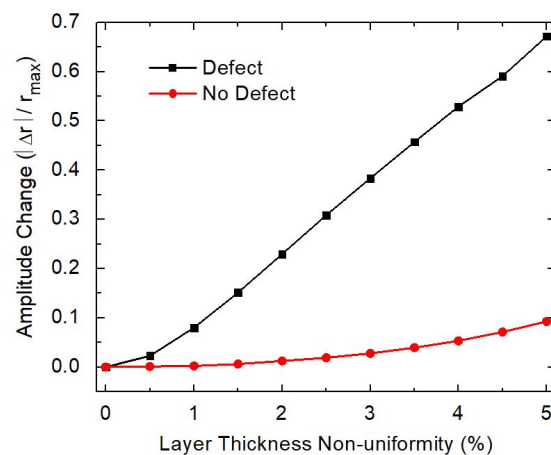


Figure 5. Amplitude change as a function of increasing layer thickness non-uniformity. The change in defect amplitude is more sensitive to changes in non-uniformity between 0% and 5% where the bandgap amplitudes of crystals without a defect experience only small changes in this range. Beyond 5% layer non-uniformity, the amplitude of the defect-mode is decreased to the point where it is no longer observed.

4. Conclusions

A one-dimensional photonic crystal with a solid, compact, defect layer was successfully fabricated via direct laser writing with two-photon polymerization. After determining and introducing one-dimensional geometric scaling factors for the low- and high-density layers, two photonic crystals were fabricated, which were identical except for the addition of a defect layer in one. For both crystals, a photonic bandgap was identified experimentally. The photonic bandgap is centered at 2500 cm^{-1} . In the photonic crystal with a defect layer, a defect mode was induced in the middle of the the photonic bandgap.

Our stratified-layer optical model calculations are in a very good agreement with the experimental results. Best-model thickness values are in a very good agreement with the

nominal design parameters. When the scaling factor (γ_{SF}) was implemented, a stratified-layer optical analysis of the reflection data from these photonic crystals reveals best-model layer thicknesses within $\pm 1.2\%$ of our nominal design values. In introducing scaling factors, we take into account not only the voxel size, but the entire effect of the two-photon polymerization, rinsing, and drying process, which results in the final geometry. Even minute changes in layer thickness non-uniformity had substantial effects on the amplitude of the defect mode. For the photonic bandgap these amplitude changes were not as pronounced. This sensitivity can be used to determine layer thickness non-uniformity in one-dimensional photonic crystals fabricated for the infrared spectral range by means of two-photon polymerization. The volumetric fill factor for the low-density layers was found to be 9.6% larger than designed. Although having minimal effects on the shape of spectral features, this change resulted in a shift of the photonic bandgap from the designed 2556 cm^{-1} to 2500 cm^{-1} . Note that the scaling factor was omitted for the volumetric fill factor, which explains the substantial deviation from its nominal value. This deviation may be reduced by introducing a separate scaling factor.

By introducing density-dependent scaling factors in the design phase we have enabled the fabrication of one-dimensional photonic crystals with defect modes which have true-to-design layer thicknesses. In contrast to determining the layer thicknesses, the interface roughness (layer thickness non-uniformity) is difficult to assess. Therefore, one-dimensional photonic crystals engineered with narrow band defect modes may provide a method to quantify this important fabrication parameter. One-dimensional photonic crystals with defect modes demonstrate features that are relevant for applications as narrow band filters [20]. In addition, photonic crystals show promise as enhanced Faraday rotators [4], omnidirectional bandgap filters [5], and sensors [18,19].

Author Contributions: Conceptualization, V.P.S., S.P. and T.H.; formal analysis, V.P.S. and T.H.; investigation, V.P.S. and T.H.; methodology, V.P.S. and M.M.; writing—original draft, V.P.S. and T.H.; writing—review and editing, S.P., M.M. and G.B. All authors have read and agreed to the published version of the manuscript.

Funding: This research was funded by the National Science Foundation (1624572) within the IUCRC Center for Metamaterials and through the National Science Foundation MRI (1828430).

Institutional Review Board Statement: Not applicable.

Informed Consent Statement: Not applicable.

Acknowledgments: The authors are grateful for support from the National Science Foundation within the IUCRC Center for Metamaterials, NSF MRI, and the Department of Physics and Optical Science of the University of North Carolina at Charlotte. V.P.S., S.P., M.M. and T.H. would like to acknowledge the valuable discussions with Darrell Childers (US Conec Ltd., Hickory, NC, USA) within the NSF IUCRC.

Conflicts of Interest: The authors declare no conflict of interest.

References

1. Yablonovitch, E. Inhibited spontaneous emission in solid-state physics and electronics. *Phys. Rev. Lett.* **1987**, *58*, 2059. [[CrossRef](#)]
2. John, S. Strong localization of photons in certain disordered dielectric superlattices. *Phys. Rev. Lett.* **1987**, *58*, 2486. [[CrossRef](#)] [[PubMed](#)]
3. Hattori, T.; Tsurumachi, N.; Nakatsuka, H. Analysis of optical nonlinearity by defect states in one-dimensional photonic crystals. *JOSA B* **1997**, *14*, 348–355. [[CrossRef](#)]
4. Steel, M.; Levy, M.; Osgood, R. High transmission enhanced Faraday rotation in one-dimensional photonic crystals with defects. *IEEE Photonics Technol. Lett.* **2000**, *12*, 1171–1173. [[CrossRef](#)]
5. Jiang, H.; Chen, H.; Li, H.; Zhang, Y.; Zhu, S. Omnidirectional gap and defect mode of one-dimensional photonic crystals containing negative-index materials. *Appl. Phys. Lett.* **2003**, *83*, 5386–5388. [[CrossRef](#)]
6. Lee, H.Y.; Yao, T. Design and evaluation of omnidirectional one-dimensional photonic crystals. *J. Appl. Phys.* **2003**, *93*, 819–830. [[CrossRef](#)]
7. Wu, C.J.; Wang, Z.H. Properties of defect modes in one-dimensional photonic crystals. *Pract. Electromagn. Res.* **2010**, *103*, 169–184. [[CrossRef](#)]
8. Tolmachev, V.A.; Baldycheva, A.V.; Berwick, K.; Perova, T.S. Influence of fluctuations of the geometrical parameters on the photonic band gaps in one-dimensional photonic crystals. *Pract. Electromagn. Res.* **2012**, *126*, 285–302. [[CrossRef](#)]

9. Rybin, M.V.; Shishkin, I.I.; Samusev, K.B.; Belov, P.A.; Kivshar, Y.S.; Kiyan, R.V.; Chichkov, B.N.; Limonov, M.F. Band structure of photonic crystals fabricated by two-photon polymerization. *Crystals* **2015**, *5*, 61–73. [[CrossRef](#)]
10. Shen, H.; Wang, Z.; Wu, Y.; Yang, B. One-dimensional photonic crystals: Fabrication, responsiveness and emerging applications in 3D construction. *RSC Adv.* **2016**, *6*, 4505–4520. [[CrossRef](#)]
11. Li, Y.; Fullager, D.; Park, S.; Childers, D.; Fesperman, R.; Boreman, G.; Hofmann, T. High-contrast infrared polymer photonic crystals fabricated by direct laser writing. *Opt. Lett.* **2018**, *43*, 4711–4714. [[CrossRef](#)]
12. Park, S.; Li, Y.; Norton, B.; McLamb, M.; Boreman, G.D.; Hofmann, T. One-dimensional Photonic Crystals Fabricated Using Stereolithographic Single Layer Assembly for the Terahertz Spectral Range. *J. Infrared Millim. Terahertz Waves* **2020**, *41*, 542–551. [[CrossRef](#)]
13. Park, S.; Li, Y.; McLamb, M.; Norton, B.; Boreman, G.D.; Hofmann, T. Highly Localized Defect Mode in Polymer-Based THz Photonic Crystals Fabricated Using Stereolithography. *J. Infrared Millim. Terahertz Waves* **2020**, *41*, 825–833. [[CrossRef](#)]
14. Sánchez, A.; Porta, A.; Orozco, S. Photonic band-gap and defect modes of a one-dimensional photonic crystal under localized compression. *J. Appl. Phys.* **2017**, *121*, 173101. [[CrossRef](#)]
15. Ahmed, A.M.; Elsayed, H.A.; Mehaney, A. High-Performance Temperature Sensor Based on One-dimensional Pyroelectric Photonic Crystals Comprising Tamm/Fano Resonances. *Plasmonics* **2021**, *16*, 547–557. [[CrossRef](#)]
16. Yablonovitch, E. Photonic crystals. *J. Mod. Opt.* **1994**, *41*, 173–194. [[CrossRef](#)]
17. Aly, A.H.; Elsayed, H.A. Defect mode properties in a one-dimensional photonic crystal. *Physica B* **2012**, *407*, 120–125. [[CrossRef](#)]
18. Wan, B.F.; Zhou, Z.W.; Xu, Y.; Zhang, H.F. A theoretical proposal for a refractive index and angle sensor based on one-dimensional photonic crystals. *IEEE Sens. J.* **2020**, *21*, 331–338. [[CrossRef](#)]
19. Nelson, R.; Haus, J. One-dimensional photonic crystals in reflection geometry for optical applications. *Appl. Phys. Lett.* **2003**, *83*, 1089–1091. [[CrossRef](#)]
20. Aly, A.H.; Elsayed, H.A.; Malek, C. Defect modes properties in one-dimensional photonic crystals employing a superconducting nanocomposite material. *Opt. Appl.* **2018**, *48*, 53–64.
21. Scotognella, F.; Chiasera, A.; Criante, L.; Aluicio-Sarduy, E.; Varas, S.; Pelli, S.; Łukowiak, A.; Righini, G.C.; Ramponi, R.; Ferrari, M. Metal oxide one dimensional photonic crystals made by RF sputtering and spin coating. *Ceram. Int.* **2015**, *41*, 8655–8659. [[CrossRef](#)]
22. Langer, R.; Barski, A.; Simon, J.; Pelekanos, N.; Konovalov, O.; Andre, R.; Dang, L.S. High-reflectivity GaN/GaN Bragg mirrors at blue/green wavelengths grown by molecular beam epitaxy. *Appl. Phys. Lett.* **1999**, *74*, 3610–3612. [[CrossRef](#)]
23. Houbertz, R.; Declerck, P.; Passinger, S.; Ovsianikov, A.; Serbin, J.; Chichkov, B. Investigations on the generation of photonic crystals using two-photon polymerization (2PP) of inorganic–organic hybrid polymers with ultra-short laser pulses. *Phys. Status Solidi A* **2007**, *204*, 3662–3675. [[CrossRef](#)]
24. Jee, H.; Park, M.J.; Jeon, K.; Jeong, C.; Lee, J. Combining Interference Lithography and Two-Photon Lithography for Fabricating Large-Area Photonic Crystal Structures with Controlled Defects. *Appl. Sci.* **2021**, *11*, 6559. [[CrossRef](#)]
25. Xing, J.F.; Zheng, M.L.; Duan, X.M. Two-photon polymerization microfabrication of hydrogels: An advanced 3D printing technology for tissue engineering and drug delivery. *Chem. Soc. Rev.* **2015**, *44*, 5031–5039. [[CrossRef](#)]
26. Tan, D.; Li, Y.; Qi, F.; Yang, H.; Gong, Q.; Dong, X.; Duan, X. Reduction in feature size of two-photon polymerization using SCR500. *Appl. Phys. Lett.* **2007**, *90*, 071106. [[CrossRef](#)]
27. Zhang, Y.L.; Chen, Q.D.; Xia, H.; Sun, H.B. Designable 3D nanofabrication by femtosecond laser direct writing. *Nano Today* **2010**, *5*, 435–448. [[CrossRef](#)]
28. Worthington, K.S.; Wiley, L.A.; Kaalberg, E.E.; Collins, M.M.; Mullins, R.F.; Stone, E.M.; Tucker, B.A. Two-photon polymerization for production of human iPSC-derived retinal cell grafts. *Acta Biomater.* **2017**, *55*, 385–395. [[CrossRef](#)] [[PubMed](#)]
29. Fullager, D.B.; Boreman, G.D.; Hofmann, T. Infrared dielectric response of nanoscribe IP-dip and IP-L monomers after polymerization from 250 cm⁻¹ to 6000 cm⁻¹. *Opt. Mater. Express* **2017**, *7*, 888–894. [[CrossRef](#)]
30. Cai, W.; Shalae, V.M. *Optical Metamaterials*; Springer: Berlin/Heidelberg, Germany, 2010; Volume 10.
31. Li, Y.; Fullager, D.; Angelbello, E.; Childers, D.; Boreman, G.; Hofmann, T. Broadband near-infrared antireflection coatings fabricated by three-dimensional direct laser writing. *Opt. Lett.* **2018**, *43*, 239–242. [[CrossRef](#)] [[PubMed](#)]